NANO LETTERS

Letter

pubs.acs.org/NanoLett

Sharp-Tip Silver Nanowires Mounted on Cantilevers for High-Aspect-Ratio High-Resolution Imaging

Xuezhi Ma,[†] Yangzhi Zhu,[‡] Sanggon Kim,[‡] Qiushi Liu,[†] Peter Byrley,[‡] Yang Wei,[∥] Jin Zhang,[∥] Kaili Jiang,[∥] Shoushan Fan,[∥] Ruoxue Yan,*[,‡,§] and Ming Liu*[,†,§]

[†]Department of Electrical and Computer Engineering, [‡]Department of Chemical and Environmental Engineering, and [§]Material Science Engineering program, Bourns College of Engineering, University of California-Riverside, Riverside, California 92521, United States

[∥]State Key Laboratory of Low-Dimensional Quantum Physics, Department of Physics and Tsinghua-Foxconn Nanotechnology Research Center, Tsinghua University, Beijing 100084, People's Republic of China

Supporting Information

ABSTRACT: Despite many efforts to fabricate high-aspect-ratio atomic force microscopy (HAR-AFM) probes for high-fidelity, high-resolution topographical imaging of three-dimensional (3D) nanostructured surfaces, current HAR probes still suffer from unsatisfactory performance, low wear-resistivity, and extravagant prices. The primary objective of this work is to demonstrate a novel design of a high-resolution (HR) HAR AFM probe, which is fabricated through a reliable, cost-efficient benchtop process to precisely implant a single ultrasharp metallic nanowire on a standard AFM cantilever probe. The force−displacement curve indicated that the HAR-HR probe is robust against buckling and bending up to 150 nN. The probes were tested on polymer trenches, showing a much better image fidelity when compared with standard silicon tips. The lateral resolution, when scanning a rough metal thin film and single-walled carbon nanotubes (SW-CNTs), was found to be better than 8 nm. Finally, stable imaging quality in tapping mode was demonstrated for at least 15 continuous scans indicating high resistance to wear. These results demonstrate a reliable benchtop fabrication technique toward metallic HAR-HR AFM probes with performance parallel or exceeding that of commercial HAR probes, yet at a fraction of their cost.

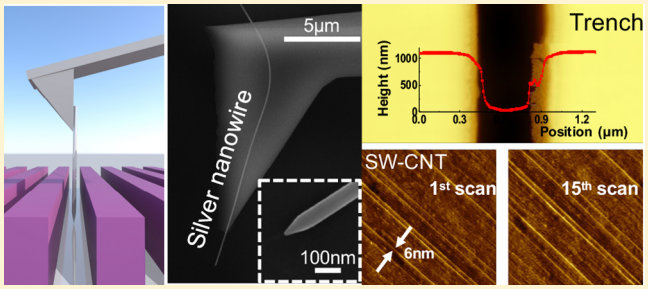

KEYWORDS: *AFM, silver nanowires, high aspect ratio, high resolution, deep trench*

With the rapid development of three-dimensional (3D) nanophotonics and nanoelectronic devices, there has been a growing demand to use atomic force microscopy (AFM) for nondestructive and rapid topographical characterization of nanostructured 3D surfaces.[1] Unlike conventional planar devices, novel 3D nanodevices, such as photonic crystals with subwavelength hole arrays[2] and fin-based multigate transistor architectures (also known as FinFETs),[3] usually have both high aspect ratios and fine lateral features. The high-aspect-ratio high-resolution (HAR-HR) topographical imaging of such 3D nanostructures then requires AFM probes with not only a small apex radius for high spatial resolution but also a high aspect ratio (>10:1) for deep trench access. Although scanning probes with intermediate aspect ratios (better than 5:1) are commercially available, the fabrication of such probes usually requires advanced nanomanufacturing techniques such as focused ion beam (FIB) deposition or focused electron beam (FEB) induced deposition,[4] leading to their extravagant prices that are 10 to 100 times higher than standard probes. Meanwhile, the limited choices of deposition materials and high density of crystal defects introduced during FIB/FEB deposition make the tips delicate and vulnerable to breakage in particular during probe approaching. In addition, the image quality deteriorates substantially even between successive scans due to low wear resistance.[5] As an alternative, carbon nanotubes (CNTs) have been attached to AFM probes for HAR-HR imaging.[6−8] However, the complicated fabrication procedures keep prices high and more importantly, limit the device success rate and reproducibility for bulk manufacturing. Therefore, HAR-HR AFM probes that can be fabricated through benchtop techniques with high performance, low cost, and good reproducibility are in urgent demand for "high fidelity" imaging of 3D nanostructures.

In parallel with CNT, another variety of HAR nanostructures that are uniquely suitable for HAR-HR AFM tips are elemental or compound nanowires. Many nanowires with aspect ratios exceeding 100:1 can be synthesized by bottom-up methods with high uniformity, low-cost, and in large scale. Also, the mechanical manipulation of nanowires is significantly easier

Received: July 7, 2016
Revised: September 18, 2016
Published: October 14, 2016

DOI: 10.1021/acs.nanolett.6b02802
Nano Lett. 2016, 16, 6896−6902

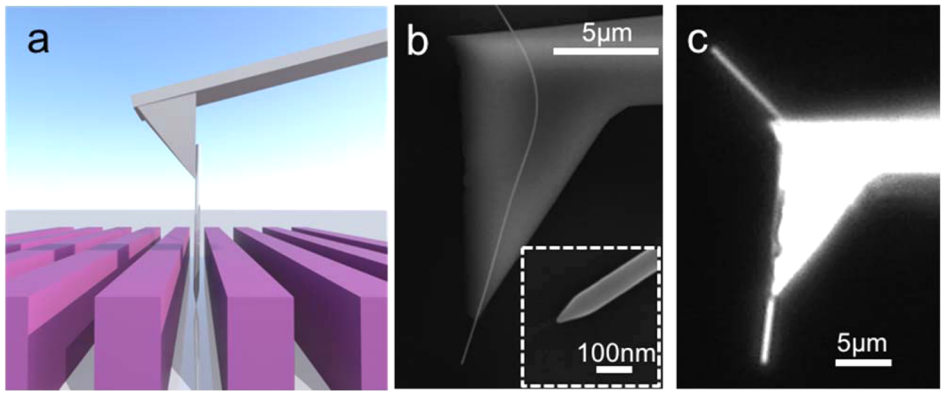

Figure 1. (a) Schematic illustration of the AgNW probe for deep-trench topographical imaging. (b) SEM image of an AgNW probe. Inset: Close-up SEM image of the sharp AgNW tip. The tip radius of the AgNW was 5 nm. (c) Dark-field optical image of the probe.

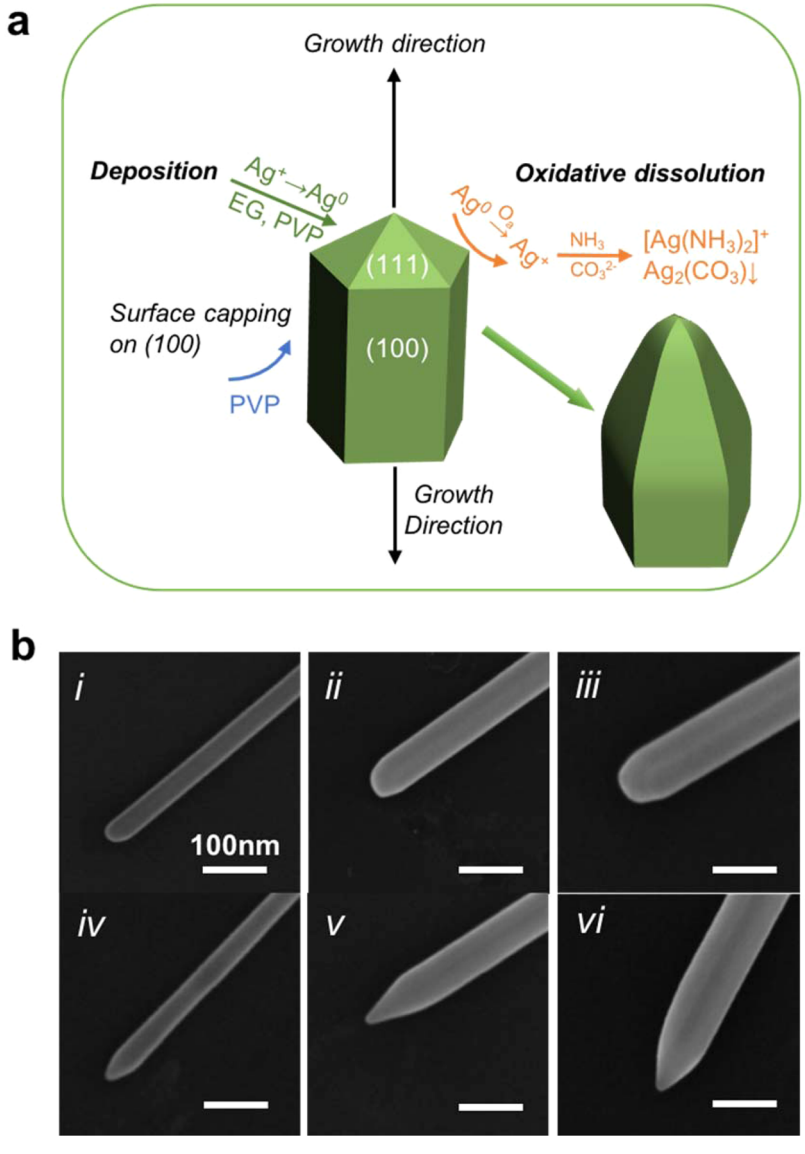

Figure 2. (a) Schematic illustration of the dynamic deposition and dissolution processes of Ag atoms at the sharpened tips of AgNWs. O_a: adsorbed O atoms. (b) SEM images of regular AgNWs (top row) and AgNWs with sharpened tips (bottom row) with different diameters. From left to right, the AgNW diameters are 40 nm (i,iv), 70 nm (ii,v) and 90 nm (iii,vi).

than CNT. For example, individual nanowires are readily distinguishable under optical microscopes and can be handled at the single-wire level with benchtop micromanipulators,[9] eliminating the fabrication requirements for slow and expensive

DOI: 10.1021/acs.nanolett.6b02802
Nano Lett. 2016, 16, 6896−6902

cleanroom processes required by CNTs-based probes. The assembly of nanowires on conventional AFM cantilevers has been previously tested as HAR-AFM probes.[10,11] However, their major drawback is the limited lateral resolution, which is dictated by the relatively large nanowire tip radius. For instance, semiconductor nanowires grown by chemical vapor deposition (CVD) via vapor−liquid−solid (VLS) methods usually have one end with rounded tip profiles[12] due to the attachment of metallic catalyst nanoparticles. Although better than the naturally flat tips of semiconductor nanowires, these catalyst particles are usually between tens to hundreds of nanometers in size, which still restrict the imaging spatial resolution. Recently, a self-assembly method to grow Ag_2Ga alloy nanowires directly on AFM cantilevers has been developed.[13] This method also creates nanowires with rounded (tip radius 25−100 nm) or even flat ends, thus still suffering from limited spatial resolution.

In this paper, we report an economical fabrication method for AFM probes that meets the requirements for both HAR and HR imaging, by integrating standard commercial AFM cantilevers with sharp-tip silver nanowires (AgNW) (tip radius down to 5 nm), which are synthesized through a low-cost, scalable, wet chemical process (Figure 1a). Figure 1b shows the scanning electron microscopy (SEM) image of the probe. The typical protruding length of the AgNW from the cantilever tip is around 3−5 μm to guarantee a high aspect ratio in the range of 40:1−70:1, as well as effectively preventing bending/buckling during approach. The sharp-tip AgNW shown in the inset of Figure 1b has a diameter ∼70 nm and tip radius of ∼8 nm.

The AgNWs used in the proposed device were synthesized with a modified polyol reduction method, which is known to produce high quality, uniform AgNWs and is scalable to keep up with industrial manufacturing needs. Such AgNWs have outstanding mechanical, electrical, and optical properties, because of their high crystallinity, low defect level, and atomically flat surfaces. These have been used in a wealth of applications from flexible/stretchable electronics[14,15] to plasmonic applications such as surface-enhanced Raman spectroscopy (SERS)[16] and subwavelength optoelectronics.[17] Compared with bulk silver, crystalline AgNWs have improved mechanical properties. Strain−stress measurements have revealed that the Young's modulus of AgNWs benefits from the stiffening size effect[18] and can reach 160 GPa,[19,20] which is 3 times larger than bulk silver and exceeds that of silicon nanowires. Although an obvious shortcoming of AgNWs is their vulnerability to oxidation, this can be mitigated by surface protective coatings, such as a thin layer of Al_2O_3 via atomic layer deposition (ALD) or a conformal Au coating through solution phase deposition.[21] Using AgNWs for HAR AFM probes is therefore applicable and to the best of our knowledge has not been reported in literature.

Aside from the many advantages outlined above, the most unique feature that sets AgNWs apart from semiconductor nanowires is their naturally pointed tips and the tunability of their tip morphologies. Chemically synthesized AgNWs are 5-fold twinned with vertical twin boundaries (TBs) meeting at the central axis of the nanowire. The 5-fold vertical twinning guides the formation of their pentagonal pyramidal ends, as illustrated in Figure 2a (SEM pictures in SI). These pointed ends are capped with five (111) facets oriented radially about the central axis of the nanowire. Each of these (111) facets has two sides in contact with its neighbors with a dihedral angle of ∼70.5°.[22] The five (111) facets join at the tip with a taper angle of ∼120° (Figure S1). Depending on the synthesis condition, the tip shape may not be rigidly polyhedron but can be rounded due to oxidative dissolution[22,23] to form an elliptical tip (Figure S1) with a tip radius of roughly half of the nanowire diameter (Figure 2b, i−iii). As an example, a nanowire with a 100 nm diameter would have a tip radius (R) of ∼50 nm.

While the pyramidal or rounded tips give these chemically synthesized AgNWs a natural advantage for high-resolution AFM imaging over semiconductor NWs with flat tips, to achieve the sub-10 nm AFM lateral resolution the AgNW tips must be further sharpened to reduce tip radii. This can be accomplished by deliberately amplifying the oxidative dissolution at the TBs between the (111) facets at the AgNW tip.[23,24] As illustrated in Figure 2a, the one-dimensional growth of AgNWs is driven by two factors: (1) the formation of seeds with multiple TBs, where significant lattice distortion, surface relaxation, and defects occur[22,25,26] to provide high-energy sites for atomic addition to feed the fast axial growth along the TBs;[22,27] and (2) the inhibition of lateral growth on the (100) side walls by capping agent poly(vinylpyrrolidone), or PVP, which binds more strongly to the (100) side surfaces, rather than with the (111) ends.[28] At the same time, the presence of air in the reaction solution could also lead to preferential oxidative dissolution or "etching" (Figure 2a, curved orange arrow) at the highly reactive TBs near the AgNW tip. This is caused by the adsorption and dissociation of molecular oxygen on the Ag surface[29−31] to form surface adsorbed oxygen atoms (O_a), which oxidize Ag^0 atoms at the nanowire surfaces and release Ag^0 back to the growth solution as Ag^+. Such oxidative etching happens preferentially at the tips due to the weak PVP binding on (111) facets and also at TBs due to their high reactivity. As a result, the original sharp edges formed by TBs between the (111) facets at the AgNW tips become rounded. By introducing coordination regents, such as NH_3 and CO_3^{2-} used in the current study, to reduce the Ag^+ concentration and drive the $Ag^0 \rightarrow Ag^+$ oxidative dissolution reaction forward, the etching effect on the tip TBs can be further amplified to form ultrasharp nanowire tips (Figure 2a). Figure 2b shows the effect of amplified oxidative etching on AgNW tip morphologies. The top panels (Figure 2b, i−iii) are AgNWs of different diameters (40, 70, and 90 nm, respectively) synthesized with conventional polyol synthesis in air. The nanowire tips are rounded due to natural oxidative etching from dissolved oxygen in the growth solution. The bottom panels (Figure 2b, iv−vi) are ultrasharp-tip AgNWs synthesized through the addition of $(NH_4)_2CO_3$ to the growth solution, while other growth parameters were kept the same. NH_4^+ dissociates to release NH_3, which then coordinates with Ag^+ to form the silver-amino complex ion $Ag(NH_3)_2^+$, while CO_3^{2-} combines with Ag^+ to form $Ag_2CO_3(s)$ due to its low solubility, both effectively reducing the Ag^+ concentration in the growth solution to accelerate the oxidative etching. The sharpening effect seen in Figure 2b (iv−vi) was consistent for AgNWs of different diameters. Figure S2 shows a series of SEM images of the ultrasharp tip AgNW sample purified through centrifugation. The purified AgNW sample was used in all subsequent AFM imaging and has a uniform diameter of 70 ± 7 nm and an average tip radius of 9 ± 5 nm.

The AgNW HAR-HR AFM probe was fabricated by adhering an AgNW onto the side wall of the pyramidical tip of a conventional silicon AFM cantilever (Olympus, Model AC160TS-R3) through a benchtop manipulation procedure that is similar to what we have previously developed.[9] First, the

DOI: 10.1021/acs.nanolett.6b02802
Nano Lett. 2016, 16, 6896−6902

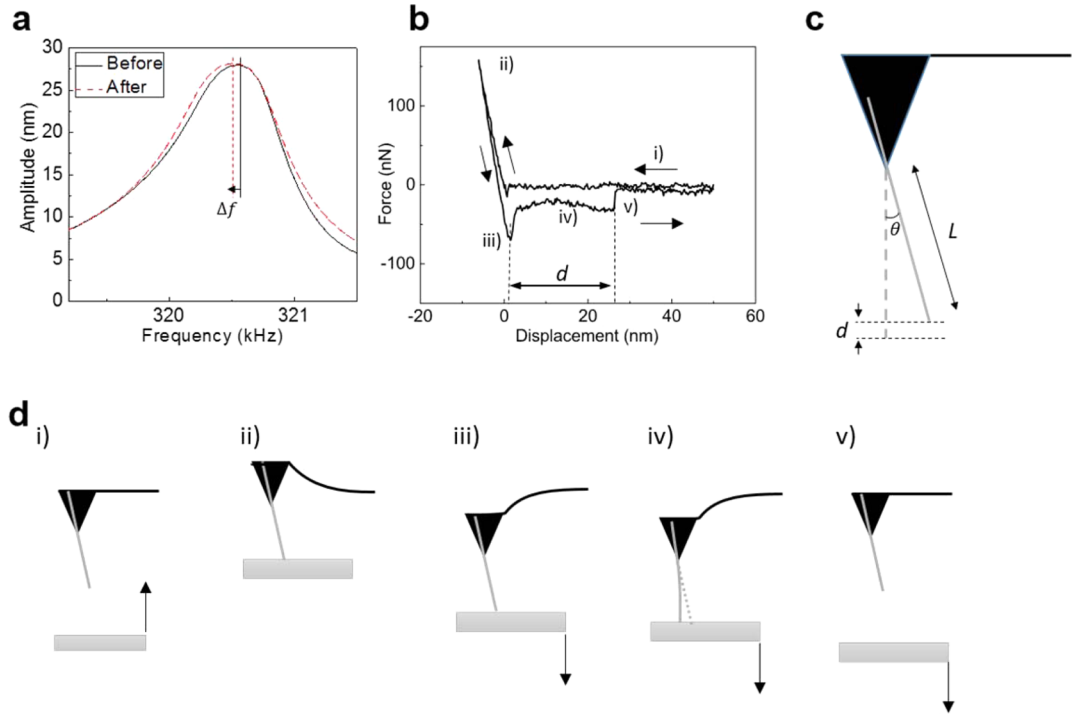

Figure 3. Mechanical characterization of an AgNW probe. (a) Frequency response curves of cantilevers before (solid black curve) and after (dashed red curve) the attachment of AgNW. (b) Force−distance curves during approach and retraction from a quartz substrate using the AgNW probe. (c,d) Schematic diagrams illustrating the probe and the proposed events during the force−distance test. (i) Substrate approaches. (ii) Cantilever bends upward. (iii) Cantilever bends downward, and the AgNW sticks to the substrate. (iv,v) The AgNW starts to slide on the substrate and pulls off.

AgNWs were dispersed onto a fresh polydimethylsiloxane (PDMS) substrate and examined with an upright optical microscope imaging system (Nikon Eclipse 80i, integrated with an Andor Zyla sCMOS Camera) to locate the AgNWs with proper lengths. Then a tungsten probe mounted on a motorized four-axis micromanipulator (MP-285, Sutter Instrument, 40 nm resolution) was used to pick up the target AgNW, place it in the desired position on the pyramidical tip, and finely adjust the protruding length by gently pushing along the nanowire. The protruding length can be controlled with a 0.5 μm accuracy, to adjust the aspect ratio of the probe to meet the measurement requirements. After the nanowire had been mounted, we used another tungsten probe to apply a small amount of epoxy glue on the AgNW-cantilever junction to improve the adhesion and prevent the detachment of AgNW during the tapping-mode measurement. Figure 1c shows a dark-field optical microscope image of an AgNW probe that is ready for measurement.

The attachment of the AgNW has little influence on the dynamic response property of the AFM cantilever. As shown in Figure 3a, the resonance frequency f only showed a marginal decrease of 0.03% (0.1 kHz) after the AgNW attachment. This result indicates that the total added mass from the AgNW and the epoxy glue ($\Delta m = m_{Ag} + m_{glue}$) is negligible compared to the effective mass (m_{eff} of the silicon cantilever. The mass of a typical AgNW is on the order of picogram, and the amount of epoxy glue applied was carefully minimized to ensure a much smaller Δm than m_{eff}, which can be derived from the resonance frequency (f) and the spring constant (k) of the cantilever via

$$f = \frac{1}{2\pi}\sqrt{\frac{k}{m_{eff}}}$$

For the cantilever used here ($k \sim 26$ N/m), m_{eff} is found to be around $6 \times 10^{-9}g$. Using the first order approximation, Δm can be derived from the change of the resonance frequency Δf, as $\Delta m = -\frac{2\Delta f}{f} m_{eff}$. For the probe measured in Figure 3a, Δm is $\sim 3 \times 10^{-12}g$, which is about 3 orders smaller than the mass of the cantilever. As a result, the performance of the cantilever can be largely maintained, as evidenced by the mechanical quality factor Q, which was reduced marginally from 307 to 281 after the AgNW adhesion.

The force−displacement curve measurement was conducted on a quartz substrate to characterize the mechanical property of the AgNW HAR-HR probe. Figure 3b shows a typical force−displacement curve during indenting and pulling of an AgNW probe with 3 μm protruding length, measured on a commercial AFM instrument (SmartSPM, AIST-NT, Inc.). When the AgNW was approaching the substrate from afar, the force curve showed a flat zero line (Figure 3b,d, i) with a tiny cantilever deflection observed near zero displacement. After the AgNW had touched the substrate, the force curve showed a linear increase up to 150 nN, at the slope of the cantilever spring constant (~26 N/m), implying that the AgNW was not bent within this range (Figure 3b,d, ii). Two detaching steps were found when the substrate was retracted from the tip. The first step (Figure 3b,d, iii) corresponded to the onset of a forward sliding motion of the AgNW tip on the substrate, as depicted in Figure 3d, iv. Because the sliding friction is smaller than the maximum static friction between the AgNW tip and the substrate, a weaker net attractive force was needed during the sliding process, which was reflected by the plateau with a smaller negative force value in Figure 3b, iv. The second step (Figure 3b,d, v) was the detachment of the bent AgNW from

DOI: 10.1021/acs.nanolett.6b02802
Nano Lett. 2016, 16, 6896−6902

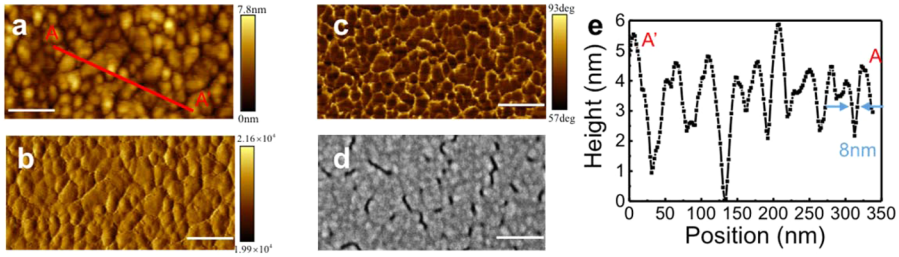

Figure 4. Tapping mode AFM topography images of a 20 nm thick gold film prepared by electron beam thermal deposition on a quartz substrate. (a−c) The height, magnitude, and phase images, respectively. (d) The SEM image of a similar region of the same sample. (e) The line cut section analysis of the marked line in (a). All scale bars are 100 nm. Imaging conditions: image resolution, 440 by 220 pixels; pixel resolution, 2 nm; scan rate, 1 Hz; cantilever oscillation amplitude, 20 nm; set-point, 87%.

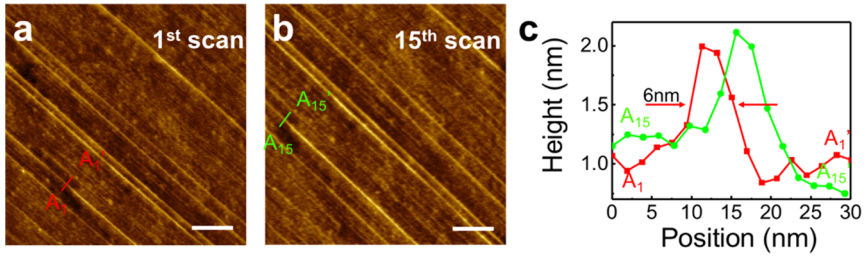

Figure 5. Continuous tapping-mode imaging of a single-walled carbon nanotube array sample on a quartz substrate. (a,b) The height images of the first and the 15th scan. Both scale bars are 100 nm. Imaging conditions: image resolution, 400 by 400 pixels; pixel resolution, 2 nm; scan rate, 1 Hz; cantilever oscillation amplitude, 20 nm; set-point, 87%. (c), Cross-sectional profiles of the SWCNT marked in (a,b).

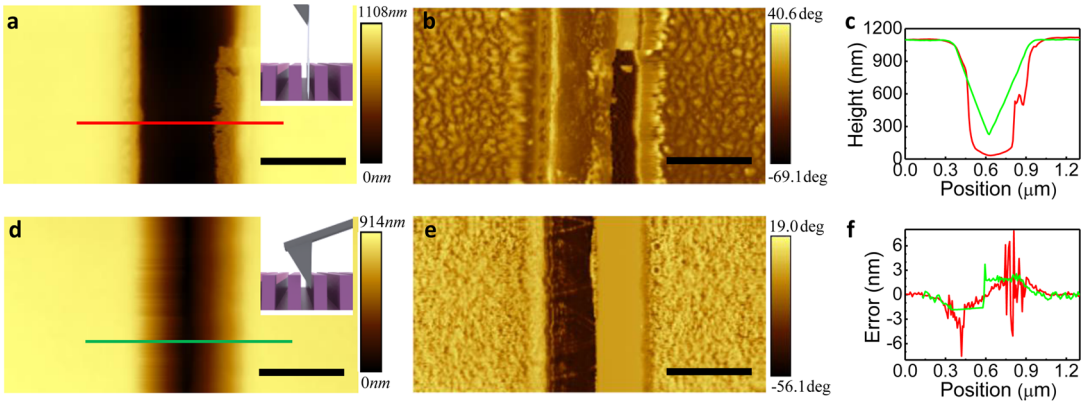

Figure 6. Comparison between an AgNW probe and a bare pyramidal silicon probe on a PMMA trench sample (trench width, 600 nm; depth, 1100 nm). (a,b) The height and the phase images acquired with the AgNW probe. (d,e) Prepared by a conventional AFM probe. Scale bars: 500 nm. (c,f) Height and error line scans. Imaging conditions: image resolution, 256 by 128 pixels; pixel resolution, 8 nm; scan rate, 1 Hz; cantilever oscillation amplitude, 20 nm; set-point, 87%.

the substrate. Assuming that the AgNW was nearly vertical at the detaching point, we can estimate the tilt angle θ from the equation $d = L(1 - \cos\theta)$, where d is the substrate displacement during the sliding process and L is the protruding length. For the probe in Figure 3, where the AgNW was aligned with the outer edge of the cantilever, θ was found to be ~7°, which is close to the tip angle of the cantilever mount. This result suggests that it is possible to further minimize the tilt angle between the AgNW and the normal vector of the substrate by choosing cantilever mounts with proper geometries.

To evaluate the spatial resolution of the AgNW HAR-HR tip, we chose a gold thin film with a rough surface as the imaging sample. The Au thin film was prepared by electron-beam thermal deposition of a 20 nm thick Au film on a silicon dioxide substrate with a 2 nm chromium (Cr) wetting layer underneath to improve the adhesion. Grains and gaps on the scale of several to tens of nanometers exist on the film surface due to the aggregation of Au atoms during the deposition, as shown in the SEM image (Figure 4d). Figure 4a-c presents the tapping mode scanning images obtained with the AgNW HAR-HR probe, corresponding to the height, magnitude, and phase images measured from the same area of the sample, respectively. The AFM images show islands and gaps with lateral dimensions that correspond well with the SEM image. The smallest gap size on the AFM image was around 8 nm.

Image reproducibility is another important benchmark to evaluate the imaging performance and longevity of AFM probes, especially for metallic AFM tips. Studies have shown that traditional metallic probes with metal coatings such as Pt, Au, and Co usually have relatively low wear resistance due to the low hardness of the sputtered metals,[32] although they are

DOI: 10.1021/acs.nanolett.6b02802
Nano Lett. 2016, 16, 6896−6902

widely needed for tip-enhanced Raman spectroscopy (TERS)[33] and covalent bonding to biomolecules for biology applications.[34] Tip wear can be reflected in the AFM data and in particular the AFM image quality.[35] Because of the high crystal quality of the chemically synthesized AgNW, the HAR-HR probe has a high wear-resistance. This can be experimentally evaluated by comparing the quality of a series of images continuously acquired from a CVD-grown single-walled carbon nanotube (CNT) sample over time.[36] As shown in Figure 5, a high spatial resolution of ~6 nm can be consistently achieved for at least 15 continuous scans, indicating excellent image reproducibility and high resistance of AgNWs to tip wear/damage.

To demonstrate the capability of the AgNW probe for high-fidelity imaging of 3D HAR samples, we fabricated a poly(methyl methacrylate) (PMMA) grating through electron beam lithography. The grating consists of 1100 nm deep, 600 nm wide trenches. Figure 6 presents the AFM images obtained using the AgNW probe and a brand new standard commercial tapping-mode AFM probe for performance comparison. The commercial AFM probe tested here was the same model as the one used to mount the AgNW (Olympus, Model AC160TS-R3), so that the specifications of the cantilevers in the two cases are identical. This comparison clearly shows that the AgNW probe delivered higher-fidelity trench images with no smearing effect on the edges that existed in the case of the commercial probe. The high aspect ratio of the AgNW probe followed the trench profile precisely (Figure 6c) and faithfully revealed the details of the trench bottom. This is particularly obvious in the phase (Figure 6b) and magnitude (Figure S5) images. The commercial probe reached only 800 nm into the trench and showed V-shaped profiles, which were the duplications of the probe cross-section.

In summary, we have demonstrated that by attaching a sharp-tip AgNW, a commercial standard AFM cantilever can be transformed into a reliable HAR-HR probe without extravagant material or fabrication costs. These sharp-tip AgNWs can be synthesized through a low-cost, scalable wet chemical synthesis with high uniformity. The fabrication process can be realized completely with economical benchtop techniques, and the additional material costs (AgNW and epoxy glue) are negligible. The fabrication process is reliable, partly due to the narrow size-distribution of the nanowires and the high-precision micromanipulation procedure. The aspect ratio of the AgNW probe is as high as 70:1, yet can be customized to meet the specific requirements of different regular or HAR samples. The performance of the AgNW HAR-HR AFM probe, including lateral and vertical spatial resolutions, wear resistance, and HAR imaging has been successfully demonstrated. The biggest obstacle that remains for the commercialization of the AgNW HAR-HR probe is the chemical stability of AgNWs in air, which limits the shelf life of the probe. AgNWs from polyol reduction synthesis are naturally coated with a thin PVP layer (1–2 nm), which can protect the surface against oxidation for up to 10 days in the air without significant decay in imaging quality. The further improvement of the probe's lifetime can be realized by applying a conformal surface antioxidation coating, such as ALD-deposited alumina or solution deposited gold. Last but not least, the AgNW supports plasmonic resonance and is a promising candidate for tip-enhanced Raman spectroscopy mapping, which adds additional functionality and value to the AgNW HAR-HR AFM probe and makes it a versatile tool for a variety of surface characterizations from topographical to chemical imaging.

■ ASSOCIATED CONTENT

Supporting Information

The Supporting Information is available free of charge on the ACS Publications website at DOI: 10.1021/acs.nanolett.6b02802.

Synthesis method and SEM images for sharp-tip AgNW and additional topographical images for SW-CNT and deep-trench samples (PDF)

■ AUTHOR INFORMATION

Corresponding Authors

*E-mail: ming@ece.ucr.edu.
*E-mail: rxyan@engr.ucr.edu.

Notes

The authors declare no competing financial interest.

■ ACKNOWLEDGMENTS

This work is supported by the UCR startup funds. X.M. and Q.L. are also supported by the UCR Seed fund.

■ REFERENCES

(1) Haugstad, G. *Atomic Force Microscopy: Understanding Basic Modes and Advanced Applications*; Wiley: New York, 2012.
(2) Priolo, F.; Gregorkiewicz, T.; Galli, M.; Krauss, T. F. *Nat. Nanotechnol.* **2014**, *9* (1), 19–32.
(3) Tang, X. H.; Bayot, V.; Reckinger, N.; Flandre, D.; Raskin, J. P.; Dubois, E.; Nysten, B.; Ieee, T. *Nanotechnology* **2009**, *8* (5), 611–616.
(4) Utke, I.; Hoffmann, P.; Melngailis, J. *J. Vac Sci. Technol. B* **2008**, *26* (4), 1197–1276.
(5) Lantz, M. A.; Wiesmann, D.; Gotsmann, B. *Nat. Nanotechnol.* **2009**, *4* (9), 586–591.
(6) Dai, H. J.; Hafner, J. H.; Rinzler, A. G.; Colbert, D. T.; Smalley, R. E. *Nature* **1996**, *384* (6605), 147–150.
(7) Burt, D. P.; Wilson, N. R.; Weaver, J. M. R.; Dobson, P. S.; Macpherson, J. V. *Nano Lett.* **2005**, *5* (4), 639–643.
(8) Wilson, N. R.; Macpherson, J. V. *Nat. Nanotechnol.* **2009**, *4* (8), 483–491.
(9) Yan, R. X.; Park, J. H.; Choi, Y.; Heo, C. J.; Yang, S. M.; Lee, L. P.; Yang, P. D. *Nat. Nanotechnol.* **2011**, *7* (3), 191–196.
(10) Christiansen, S. H.; Becker, M.; Fahlbusch, S.; Michler, J.; Sivakov, V.; Andra, G.; Geiger, R. *Nanotechnology* **2007**, *18* (3), 035503.
(11) Engstrom, D. S.; Savu, V.; Zhu, X. N.; Bu, I. Y. Y.; Milne, W. I.; Brugger, J.; Boggild, P. *Nano Lett.* **2011**, *11* (4), 1568–1574.
(12) Dasgupta, N. P.; Sun, J. W.; Liu, C.; Brittman, S.; Andrews, S. C.; Lim, J.; Gao, H. W.; Yan, R. X.; Yang, P. D. *Adv. Mater.* **2014**, *26* (14), 2137–2184.
(13) Yazdanpanah, M. M.; Harfenist, S. A.; Safir, A.; Cohn, R. W. *J. Appl. Phys.* **2005**, *98* (7), 073510.
(14) Hu, L. B.; Kim, H. S.; Lee, J. Y.; Peumans, P.; Cui, Y. *ACS Nano* **2010**, *4* (5), 2955–2963.
(15) Garnett, E. C.; Cai, W. S.; Cha, J. J.; Mahmood, F.; Connor, S. T.; Christoforo, M. G.; Cui, Y.; McGehee, M. D.; Brongersma, M. L. *Nat. Mater.* **2012**, *11* (3), 241–249.
(16) Lu, G.; De Keersmaecker, H.; Su, L.; Kenens, B.; Rocha, S.; Fron, E.; Chen, C.; Van Dorpe, P.; Mizuno, H.; Hofkens, J.; Hutchison, J. A.; Uji-i, H. *Adv. Mater.* **2014**, *26* (30), 5124–5128.
(17) Fang, Y. R.; Li, Z. P.; Huang, Y. Z.; Zhang, S. P.; Nordlander, P.; Halas, N. J.; Xu, H. X. *Nano Lett.* **2010**, *10* (5), 1950–1954.
(18) Calahorra, Y.; Shtempluck, O.; Kotchetkov, V.; Yaish, Y. E. *Nano Lett.* **2015**, *15* (5), 2945–2950.

DOI: 10.1021/acs.nanolett.6b02802
Nano Lett. 2016, 16, 6896–6902

(19) Narayanan, S.; Cheng, G. M.; Zeng, Z.; Zhu, Y.; Zhu, T. *Nano Lett.* **2015**, *15* (6), 4037−4044.
(20) Zhu, Y.; Qin, Q. Q.; Xu, F.; Fan, F. R.; Ding, Y.; Zhang, T.; Wiley, B. J.; Wang, Z. L. *Phys. Rev. B: Condens. Matter Mater. Phys.* **2012**, *85* (4), 045443.
(21) Gao, C. B.; Lu, Z. D.; Liu, Y.; Zhang, Q.; Chi, M. F.; Cheng, Q.; Yin, Y. D. *Angew. Chem., Int. Ed.* **2012**, *51* (23), 5629−5633.
(22) Wiley, B.; Herricks, T.; Sun, Y. G.; Xia, Y. N. *Nano Lett.* **2004**, *4* (9), 1733−1739.
(23) Korte, K. E.; Skrabalak, S. E.; Xia, Y. N. *J. Mater. Chem.* **2008**, *18* (4), 437−441.
(24) Liu, S. H.; Sun, B. M.; Li, J. G.; Chen, J. L. *CrystEngComm* **2014**, *16* (2), 244−251.
(25) Hofmeister, H.; Nepijko, S. A.; Ievlev, D. N.; Schulze, W.; Ertl, G. *J. Cryst. Growth* **2002**, *234* (4), 773−781.
(26) Nepijko, S. A.; Ievlev, D. N.; Schulze, W.; Urban, J.; Ertl, G. *ChemPhysChem* **2000**, *1* (3), 140.
(27) Gai, P. L.; Harmer, M. A. *Nano Lett.* **2002**, *2* (7), 771−774.
(28) Sun, Y. G.; Mayers, B.; Herricks, T.; Xia, Y. N. *Nano Lett.* **2003**, *3* (7), 955−960.
(29) Campbell, C. T. *Surf. Sci.* **1985**, *157* (1), 43−60.
(30) deMongeot, F. B.; Cupolillo, A.; Valbusa, U.; Rocca, M. *Chem. Phys. Lett.* **1997**, *270* (3−4), 345−350.
(31) Sexton, B. A.; Madix, R. J. *Chem. Phys. Lett.* **1980**, *76* (2), 294−297.
(32) Chung, K. H. *Int. J. Precis Eng. Man* **2014**, *15* (10), 2219−2230.
(33) Huth, F.; Chuvilin, A.; Schnell, M.; Amenabar, I.; Krutokhvostov, R.; Lopatin, S.; Hillenbrand, R. *Nano Lett.* **2013**, *13* (3), 1065−1072.
(34) Lee, K. B.; Lim, J. H.; Mirkin, C. A. *J. Am. Chem. Soc.* **2003**, *125* (19), 5588−5589.
(35) Liu, J. J.; Notbohm, J. K.; Carpick, R. W.; Turner, K. T. *ACS Nano* **2010**, *4* (7), 3763−3772.
(36) He, Y. J.; Zhang, J.; Li, D. Q.; Wang, J. T.; Wu, Q.; Wei, Y.; Zhang, L. N.; Wang, J. P.; Liu, P.; Li, Q. Q.; Fan, S. S.; Jiang, K. L. *Nano Lett.* **2013**, *13* (11), 5556−5562.

DOI: 10.1021/acs.nanolett.6b02802
Nano Lett. 2016, 16, 6896−6902